Thermo-Optical Parameters of Amorphous a-C:N:H Layers

E. Pieczyńska[a], J. Jaglarz[b], K. Marszalek[a] and K. Tkacz-Śmiech[a,*]
[a]AGH University of Science and Technology, al. A. Mickiewicza 30, 30-059 Kraków, Poland
[b]Cracow Technical University, Podchorążych 1, 30-084 Kraków, Poland

(Received April 3, 2014)

Thermo-optical properties of hydrogenated amorphous carbon nitride layers (a-C:N:H) deposited on crystalline silicon by plasma assisted chemical vapour deposition were studied. The layers were characterized by the Fourier transform infrared spectroscopy and their chemical composition, i.e. [N]/[C] ratio, was determined by energy dispersive X-ray technique. The optic measurements were made by spectroscopic ellipsometer Wollam M2000 equipped with a heated vacuum chamber. The measurements of ellipsometric angles were carried out during heating the sample from room temperature to 300 °C. Refractive index, extinction coefficient and the layer thicknesses were calculated by fitting the model of the layer to the ellipsometric data. The results confirm that at about 23 °C the layer properties are changed. The measured thermo-optical parameters, $\mathrm{d}n/\mathrm{d}T$ and $\mathrm{d}k/\mathrm{d}T$, show abrupt change from negative to positive values which can be explained by structure graphitization. Simultaneously, the bandgap decreases from 2.5 to 0.7 eV and the layer thickness drops to about 50% of the initial value.

DOI: 10.12693/APhysPolA.126.1241
PACS: 07.60.Fs, 78.20.–e, 78.20.Ci, 78.20.N–, 78.30.Ly, 81.05.U–, 81.15.Gh

1. Introduction

A research in technology and characterisation of amorphous carbon nitride layers has been provoked by a worldwide interest to synthesise extremely hard stoichiometric crystalline β-C_3N_4. According to theoretical predictions such crystals should have elastic modulus and hardness higher than diamond [1]. Despite much research, the β-C_3N_4 phase was not synthesised. Instead, good properties of nonstoichiometric amorphous carbon nitride, a-C:N, and hydrogenated carbon nitride layers, a-C:N:H, were discovered. Such layers exhibit good tribological properties and high corrosion resistance which makes them attractive material for protective coatings in machinery industry, medicine and implantology [2–4]. Good properties and high stability of carbon nitride layers make them more and more often replacing carbon layers. The carbon nitride layers have an advantage over amorphous carbon because of good adhesion to the substrate. Such effect is achieved thanks to nitrogen admixture which relaxes the structure and reduces internal stresses [5–7].

The utility parameters of carbon nitride layers depend on their chemical composition, i.e. C, N and possibly H content, and atomic structure. In most works, a fraction of carbon in various hybridisation, C-sp^2 or C-sp^3 phase, is considered as a main structure parameter which has a crucial impact on the layer properties. It depends on the nitrogen content and can be various in the layers obtained by various technologies or just at various conditions using the same method. The structure of the layer with predominant C-sp^2 fraction can be imagined as a network of crosslinking graphite-like clusters. The properties of such layers differ from the properties of the layers in which C-sp^3 fraction dominates.

Depending on the atomic structure and the ratio of sp^2 to sp^3 bonded carbon, the carbon nitride layers are classified into following types [8, 9]:

- a-C:N layers with high C-sp^2 fraction in which more than 70% of carbon resides in sp^2 sites;
- ta-C:N layers with high fraction of C-sp^3 (80÷90%) and nitrogen content about 10% and below. When the nitrogen content exceeds 10% then the C-sp^3 fraction and the layer density rapidly decrease.

The hydrogenated layers are classified in a similar way. One distinguishes:

- a-C:N:H layers with a moderate C-sp^3 and low N contents;
- ta-C:N:H layers with the C-sp^3 fraction exceeding 60%, nitrogen content up to 20% and a meaningful hydrogen content (about 30% and more).

In this work we focus on a-C:N:H layers fabricated by plasma assisted chemical vapour deposition (PACVD) technique on (001)-oriented silicon. Despite much research concerning properties of such layers little is known about their optical properties and this has become an inspiration for the current studies.

We present, for the first time, the results of measurements of thermo-optical parameters of a-C:N:H layers. The temperature dependences of refraction index and extinction coefficient are measured by spectroscopic ellipsometry at the temperatures gradually rising from room temperature to 300 °C. Because the applied method is still infrequently used in the studies of the layers and surfaces, the paper has become a pretext to outline theoretical basis and experimental details of the method.

*corresponding author; e-mail: smiech@agh.edu.pl

2. Determination of thermo-optical parameters

The dispersion dependences of optical constants of layers and coatings can be measured by spectroscopic ellipsometry. In the method, two angles, Ψ and Δ, are measured at various wavelengths [10]. The angle Ψ is given by the ratio of the squares of complex Fresnel coefficients, r_p and r_s, for "p" and "s" polarizations

$$\tan\Psi = |r_p|^2 / |r_s|^2 . \tag{1}$$

Δ is a phase shift between the polarized waves

$$r_p/r_s = \exp(i\Delta)\tan\Psi. \tag{2}$$

When Ψ and Δ are known then the refractive index n, extinction coefficient k, and roughness σ of the layer can be calculated.

An amorphous layer can be described by the extended Cauchy model, within which dispersion relations are formulated. For slightly absorbing layer, the indices n and k are [11]:

$$n(\lambda) = A + \frac{B}{\lambda^2} + \frac{C}{\lambda^4} \tag{3}$$

$$k(\lambda) = k\exp\left[\eta\left(\frac{\mathrm{hc}}{\lambda} - E_{\mathrm{bandedge}}\right)\right], \tag{4}$$

where A, B, C and η are constants, and k and E_{bandedge} are matched parameters which describe Urbach absorption tail [12].

Thermo-optical coefficients (TOC), $\mathrm{d}n/\mathrm{d}T$ and $\mathrm{d}k/\mathrm{d}T$, determine temperature dispersion of refractive index and extinction coefficient.

According to Prod'homme theory [13, 14], $\mathrm{d}n/\mathrm{d}T$ depends on two factors. One is a volume expansion coefficient, $\beta = \frac{1}{V_0}\frac{\mathrm{d}V}{\mathrm{d}T}$, and the other is an electronic polarizability coefficient, $\Phi = \frac{1}{P}\frac{\mathrm{d}P}{\mathrm{d}T}$ (P is polarization):

$$\frac{\mathrm{d}n}{\mathrm{d}T} = f(n)(\Phi - \beta), \tag{5}$$

where $f(n)$ is given by

$$f(n) = \frac{(n^2-1)(n^2+2)}{6n}. \tag{6}$$

If the polarizability term in (5) is dominant, then the refractive index increases with the temperature and $\frac{\mathrm{d}n}{\mathrm{d}T}$ is positive. TOC is negative when the thermal expansion term is prevailing.

3. Experiment

3.1. Sample preparation

The a-C:N:H layers were deposited by RF PACVD method in which plasma is generated by 13.56 MHz field (radio frequency — RF). In this method, the deposition occurs as a byproduct of chemical reactions initiated by neutral collisions with the non-equilibrium energetic electrons produced by RF plasma, instead of thermal energy. The deposition precursors in such case are produced at much lower temperatures than in classical thermal CVD.

The layers used in the present studies were deposited on crystalline silicon wafers c-Si (001) at the process carried out without heating. Silicon was chosen as a substrate due to its sharp optical differences on a film-substrate interface. The processing temperature was 45 °C. Before starting the process, the silicon wafers were washed with acetone and isopropyl alcohol. Directly before layer deposition the substrates were subjected to 10 min etching in argon plasma. The other processing parameters are specified in Table.

TABLE

CVD — processing parameters.

		Etching	Deposition
reactor		RF PACVD	
field/frequency [MHz]		radio waves; 13.56	
power [W]		60	
pressure [Tr], [Pa]		0.4; 53.3	
substrate		c-Si (001) oriented	
substrate temperature [°C]		45	
substrate surface [cm^2]		4	
time [min]		10	110
gaseous substrates		Flow [cm^3/min]	
	Ar	200	75
	CH_4	–	10
	N_2	–	100

3.2. Chemical composition and atomic structure

The chemical composition of the layer was roughly estimated by EDX technique (Nova Nano SEM 200 FEI with EDX analysis). The results confirm that the a-C:N:H layer with [N]/[C]≈ 0.3 was deposited. The SEM image of the layer is typical for amorphous layers of good quality (Fig. 1).

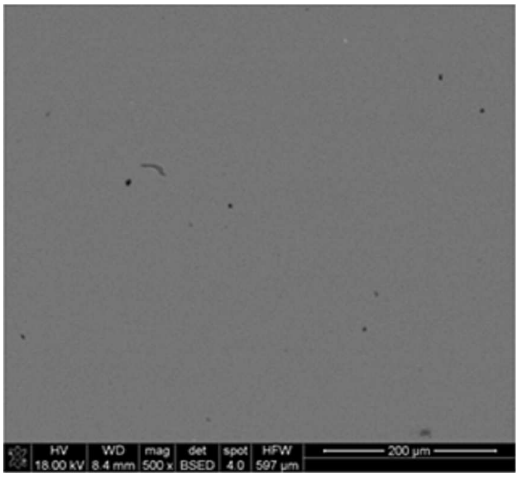

Fig. 1. SEM image of the a-C:N:H layer deposited on c-Si (001) wafer. The chemical composition measured from the visible area is: C: 45.5 at.%, N: 12.1 at.%, Si: 42.49 at.% (signal from the substrate); [N]/[C]≈ 0.3.

The atomic structure of the layer was characterised on the basis of the FTIR spectrum measured within 400 ÷ 4000 cm^{-1} by BIO-RAD FTS60V (resolution 4 cm^{-1}, 275 scans). The recorded spectrum is shown in Fig. 2. It presents a profile typical for a-C:N:H layers with visible four absorption regions at: 2750÷3500 cm^{-1}, 2000÷2350 cm^{-1}, 1000÷2000 cm^{-1} and the peaks below 1000 cm^{-1}, located in so-called fingerprint region [15–23].

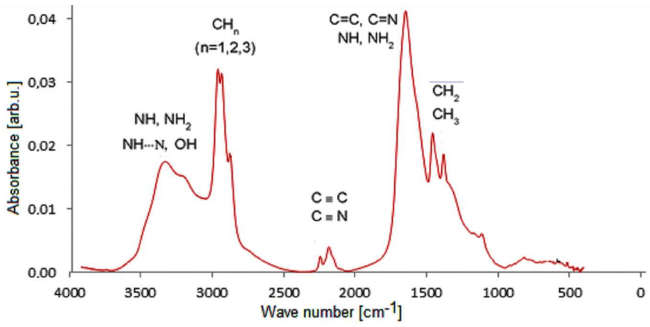

Fig. 2. FTIR spectrum of the a-C:N:H layer deposited on c-Si wafer.

The absorption within 3250÷3500 cm^{-1} wave numbers is characteristic for the stretching of NH terminal groups. Its manifestation confirms a presence of hydrogen-bonded nitrogen, characteristic for highly polymeric a-C:N:H layers. The entire band may be considered as the result of overlapping of the peaks due to stretching vibrations in primary and secondary amine groups. The band between 2750 and 3250 cm^{-1} is an effect of overlapping of the modes due to CH symmetric and asymmetric stretching in $\equiv$CH, $=CH_2$ and $-CH_3$ groups with *sp*, sp^2 or sp^3 carbon — in the sequence of increasing wave number. The broad band between 3200 and 3500 cm^{-1} can be assigned to the OH groups adsorbed from the atmosphere and to the oscillations of hydrogen bridges between the nitrogen atoms. The weak absorption observed within 2000÷2350 cm^{-1} is typically attributed to the vibrations of double or triple bonds between carbon and nitrogen.

The assignment of the intense band located between 1000 and 1900 cm^{-1} requires more attention and despite much research remains controversial. A detailed assignment of the vibrations active within this region has been mainly based on the pioneering paper by Kaufman et al. [20]. It was claimed in this work that the absorption between 1000 and 1900 cm^{-1} could be related to the D and G Raman peaks which became IR active due to breaking of sp^2 domains symmetry by nitrogen. Such explanation is currently considered as a confusing one. As noticed by Robertson et al., the absorption band recorded between 1000 and 1900 cm^{-1} for carbon nitride layers resembles the absorption band in this region for N-free amorphous carbon where symmetry is not broken [9, 21–23].

In fact, the CN absorption is observed at the same region as the CC mode, i.e. at 1500 ÷ 1600 cm^{-1} for sp^2 and 1300 ÷ 1600 cm^{-1} for sp^3 ring species. A well-defined peak at 1599 cm^{-1} is likely due to C=N or C=C in graphitic-like structures. It overlaps with the band assigned to NH bending (conjugated with the stretching band at about 3300 cm^{-1}). The C–N polar bonds merely contribute spectrum.

The effect of nitrogen incorporation on the structure of the layers can be summarized as follows. Nitrogen breaks the electronic symmetry of π rings and increases a charge localised at C, likewise in C–C bonds. It also encourages sp^2 bonding, promotes clustering and facilitates interlayer bonding. When C is substituted by N then one π bond is broken. An unpaired electron can form a σ bond with similar electron from the adjacent layer, leading to the formation of diamond-like clusters. It can also cause the structure curling and disorder confirmed by the strong absorption observed around 1320 cm^{-1}.

3.3. Optical and thermo-optical properties

The spectra of Ψ and Δ ellipsometric angles were recorded in the range 200 ÷ 1700 nm by M-2000 ellipsometer (Woollam Co.). The measurements were repeated for three angles of incidence: 60°, 65° and 70°. The data were analyzed using CompleteEASE 5.0 software. The dispersion curves of Ψ, Δ measured at 25 °C and at 300 °C are shown in Fig. 3 but the spectral dependences were measured in the whole temperature range, i.e. from 25 °C to 300 °C every 10 deg. The Cauchy model of the layer was fitted to the experimental data and the fitted dependences are represented by dashed lines in Fig. 3. It is seen that very good agreement has been achieved [24].

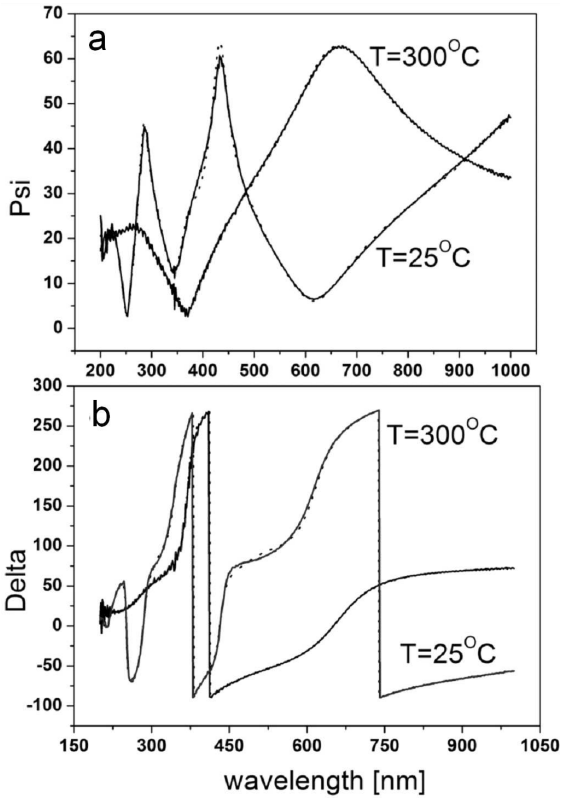

Fig. 3. The spectra of ellipsometric angles: (a) $\Psi(\lambda)$, (b) $\Delta(\lambda)$ determined for the a-C:N:H layer deposited on Si(001) wafer. The results measured at 25 °C and 300 °C. Solid line — experiment, dashed line — the Cauchy model fitting.

The fitted $\Psi(\lambda)$ and $\Delta(\lambda)$ dependences were used in calculations of the dispersion relations of the refractive index and extinction coefficient. The results of calculations are shown in Fig. 4. It is clearly seen that the results

for 25 °C and 300 °C differ. The refractive index measured at 300 °C increases from 1.53 at 200 nm to about 1.65 at 380 nm. For longer waves it decreases and shows normal dispersion. At room temperature, normal dispersion is observed in the whole spectral range.

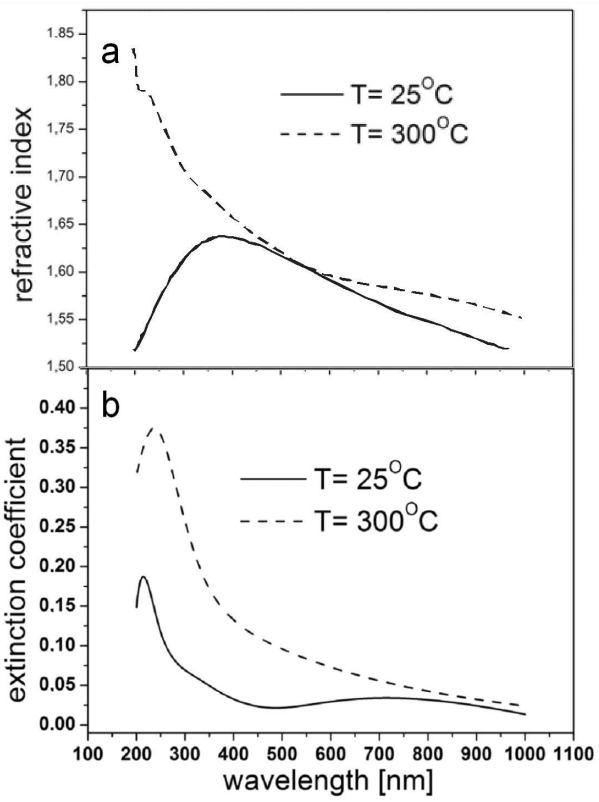

Fig. 4. Dispersion of refractive index (a) and extinction coefficient (b) of the a-C:N:H layer deposited on silicon substrate. The results measured at 25 °C and 300 °C.

Similar fitting was made for the results obtained at various temperatures. Hence, temperature dependences of n and k were generated and the layer thicknesses calculated. The results are shown in Figs. 5 and 6.

The temperature dispersion of n and k at $\lambda = 633$ nm is presented in Fig. 5. It is seen that both $\mathrm{d}n/\mathrm{d}T$ and $\mathrm{d}k/\mathrm{d}T$ are negative up to about 230 °C. Above this temperature, up to about 280 °C, the refractive index and extinction coefficient increase with rising temperature. Such result means that at about 230 °C the structure of the layer could change.

For certainty, the layer thicknesses at various temperatures were compared (Fig. 6). The results show that the layer thickness, initially 227 nm, does not change up to 230 °C but above this temperature it dramatically goes down to 124 nm. A rapid decrease of the thickness correlates with the changes of thermo-optical coefficients.

Further knowledge concerning a transformation of the structure of the layer was obtained from a comparison of a bandgap of the layer at room temperature with the bandgap determined for the layer heated to 300 °C.

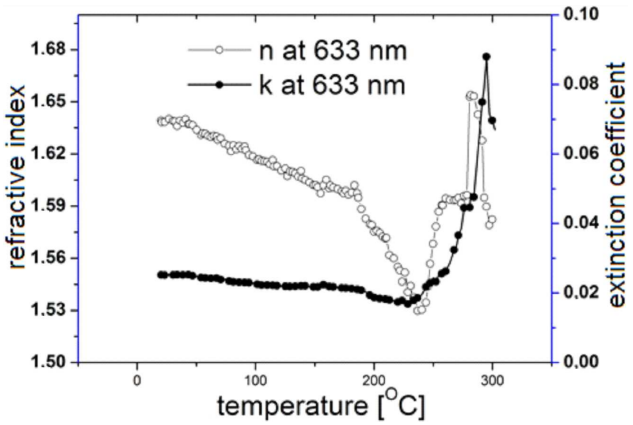

Fig. 5. Temperature dispersion of refractive index and extinction coefficient of the a-C:N:H layer deposited on Si (001) substrate.

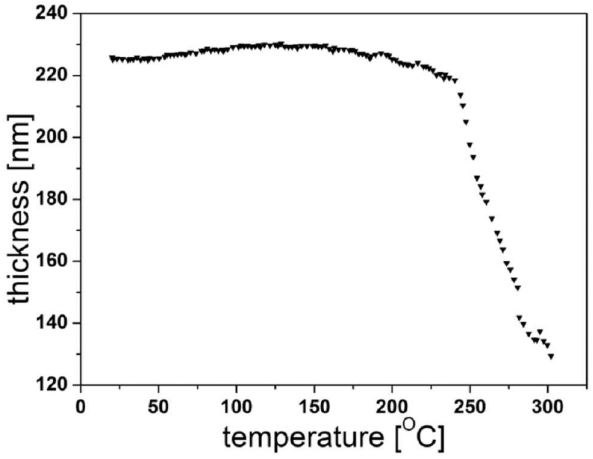

Fig. 6. Temperature dependence of the thickness of the a-C:N:H layer deposited on Si (001).

The optical absorption behaviour of the layer at the absorption edge was interpreted with a use of empirical Tauc–Lorentz model which is a convenient way to parametrize the optical functions of amorphous materials [25]. The results of fitting the Tauc plot (dashed line) to the results obtained from ellipsometric measurements (solid line) are shown in Fig. 7. From the fitted curve the optical gap of the layer at room temperature and at 300 °C was evaluated. The respective values are: 2.455 eV for the sample at room temperature and 0.72 eV for the sample heated up to 300 °C.

The observed change of the bandgap can be due to partial graphitization of the layer structure. According to [9] such narrowing of the band gap involves increase of the sp^2-phase fraction from about 0.2 to $0.5 \div 0.7$. The graphitization can be accompanied by gradual hydrogen release.

4. Summary

The obtained results are very important for technology and application of a-C:N:H layers. The sharp decrease of the layer thickness observed for the sample heated

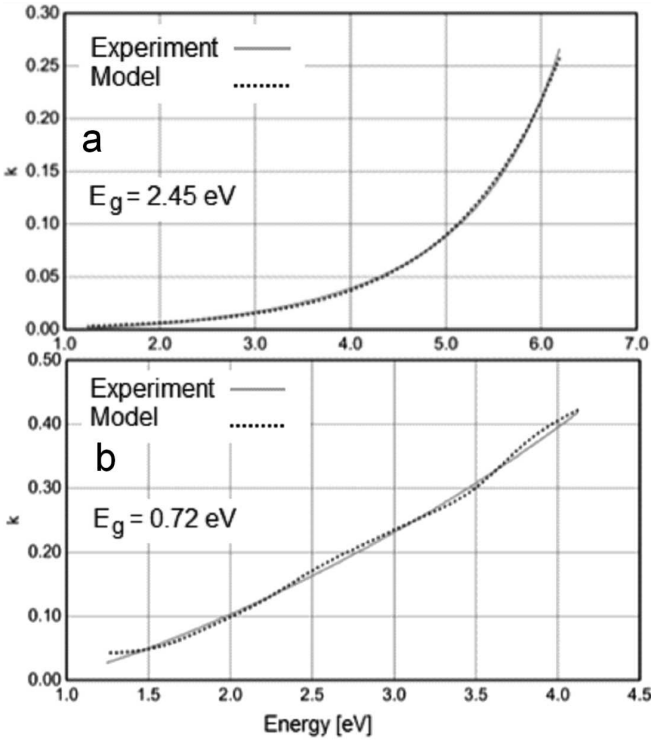

Fig. 7. Spectral dependence of extinction coefficient for a-C:N:H layer (solid line) together with the fitted Tauc plot (dashed line). The data for the sample at room temperature (a) and for the sample heated up to 300 °C (b).

above 230 °C can be explained by a transformation of the structure of the layer. The changes of the thermo-optical coefficients, from negative to positive values, give additional evidence for such transformation. An accompanying change of the bandgap from 2.5 eV at room temperature to 0.7 eV above 230 °C suggests that there has been structure graphitization, from about 20% of the C-sp^2-phase fraction at low temperatures to $0.5 \div 0.7$ of C-sp^2 above 230 °C, accompanied by partial hydrogen releasing.

Acknowledgments

The paper was financially supported by European Union from the sources of the European Regional Development Fund for 2007–2013, the Innovative Economy Operational Programme Priority Axis 1 — Research and development of state-of-the-art technologies, Project POIG.01.03.01-30-056/12.

References

[1] Y. Liu, M.L. Cohen, *Science* **245**, 841 (1989).

[2] Y.S. Zou, Y.F. Wu, R.F. Huang, C. Sun, L.S. Wen, *Vacuum* **83**, 1406 (2009).

[3] D.F. Wang, K. Kato, N. Umehara, *Surf. Coat. Technol.* **123**, 177 (2000).

[4] C.A. Charitidis, *Int. J. Ref. Metal. Hard Mater.* **28**, 51 (2010).

[5] H.R. Aryal, S. Adhikari, S. Adhikary, H. Uchida, M. Umeno, *Diam. Relat. Mater.* **15**, 1906 (2006).

[6] N. Dwivedi, S. Kumar, H.K. Malik, C.M.S. Rauthan, O.S. Panwar, *Mater. Chemistry & Physics* **130**, 775 (2011).

[7] S.R.P. Silva, J. Robertson, G.A.J. Amaratunga, B. Rafferty, L.M. Brown, J. Schwan, D.F. Franceschini, G. Mariotto, *J. Appl. Phys.* **81**, 2626 (1997).

[8] C. Casiraghi, J. Robertson, A.C. Ferrari, *Mater. Today* **10**, 44 (2007).

[9] A.C. Ferrari, S.E. Rodil, J. Robertson, *Phys. Rev. B* **67**, 155306 (2003).

[10] R.M.A. Azzam, N.M. Bashara, *Ellipsometry and Polarized Light*, North-Holland, Amsterdam 1995.

[11] K. Marszalek, P. Winkowski, J. Jaglarz, *Mater. Sci.-Poland* **32**, 80 (2014).

[12] *Complete EASE™ Data Analysis Manual*, v.4.05, J.A. Woollam Co. Inc., 2009.

[13] F. Urbach, *Phys. Rev.* **92**, 1324 (1953).

[14] S.V. Kartalopoulos, *Introduction to DWDM Technology*, SPIE Press, Bellingham (WA) 2000, p. 141.

[15] P. Jedrzejowski, J. Cizek, A. Amassian, J.E. Klemberg-Sapieha, J. Vlcek, L. Martinu, *Thin Solid Films* **447-448**, 201 (2004).

[16] K. Kyziol, S. Jonas, K. Tkacz-Smiech, K. Marszalek, *Vacuum* **82**, 998 (2008).

[17] Y. Awad, M.A.E. Khakani, C. Aktik, J. Mouine, N. Camire, M. Lessard, M. Scarlete, *Surf. Coat. Technol.* **204**, 539 (2009).

[18] K.B. Sundarm, J. Alizadeh, *Thin Solid Films* **370**, 151 (2000).

[19] J.H. Kaufman, S. Metin, D.D. Saperstein, *Phys. Rev. B* **39**, 13053 (1989).

[20] S.E. Rodil, N.A. Morrison, J. Robertson, W.I. Milne, *Phys. Status Solidi A* **174**, 25 (1999).

[21] G. Lazar, K. Zellamaa, I. Vascan, M. Stamate, I. Lazar, I. Rusu, *J. Optoel. Adv. Mater.* **7**, 647 (2005).

[22] A.C. Ferrari, S.E. Rodil, J. Robertson, *Diam. Relat. Mater.* **12**, 905 (2003).

[23] S.E. Rodil, A.C. Ferrari, J. Robertson, S. Muhl, *Thin Solid Films* **420**, 122 (2002).

[24] J. Jaglarz, M. Kepinska, J. Sanetra, *Opt. Mater.* **36**, 1275 (2014).

[25] A. Ibrahim, S.K.J. Al-Ani, *Czech. J. Phys.* **44**, 785 (1994).